RSC Advances

PAPER

View Article Online
View Journal | View Issue



Cite this: *RSC Adv.*, 2014, **4**, 61012

# Solvent-tuning of ordered mesoporous silicas prepared through evaporation-induced self-assembly templated by poly(ethylene oxide-*b*-ε-caprolactone)

Wei-Cheng Chu, Chen-Xin Lin and Shiao-Wei Kuo*

Received 30th September 2014
Accepted 6th November 2014

DOI: 10.1039/c4ra11569d

www.rsc.org/advances

In this study, we employed the diblock copolymer poly(ethylene oxide-*b*-ε-caprolactone (PEO-*b*-PCL, $EO_{114}CL_{84}$) as a template to prepare mesoporous silica materials while controlling the tetraethyl orthosilicate (TEOS)-to-PEO-*b*-PCL ratio and testing the effects of various solvents [$CH_2Cl_2$, tetrahydrofuran (THF), acetone]. Small-angle X-ray scattering, transmission electron microscopy, and $N_2$ adsorption/desorption isotherms revealed that the mesostructures of these mesoporous silicas were influenced by the TEOS content and the solvent. Acetone was superior to $CH_2Cl_2$ and THF as the solvent when forming more-ordered mesostructures through evaporation-induced self-assembly (EISA), with the degree of the ordered structure increasing upon increasing the TEOS–to–PEO-*b*-PCL ratio. In addition, we obtained a long-range-ordered body-centered cubic (bcc) mesoporous structure through the EISA process when the TEOS/PEO-*b*-PCL ratio was 5 : 1 in acetone; such structures did not form when $CH_2Cl_2$ or THF were the solvents. Because the concentration of the template during the EISA process depended on the solvent evaporation rate and solubility, we could prepare highly ordered mesoporous silicas having narrow pore size distributions and various morphologies merely through selection of an appropriate solvent.

## Introduction

Mesoporous silicas are applied widely because of their high thermal stability, high volume fractions, and high surface areas. Their first syntheses were reported by Mobil scientists who used cationic surfactants [*e.g.*, cetyltrimethylammonium bromide (CTAB)] as templates to obtain highly ordered mesoporous molecular sieves (MCM-41s).[1,2] Subsequently, many studies have been conducted to investigate the formation of mesostructures using low-molecular-weight block copolymers as templates through precipitation-based methods (SBA-*n*).[3–6] Application of this approach was, however, limited because the low-molecular-weight block copolymers used as templates are soluble only in aqueous systems. Accordingly, a dominant synthetic strategy was developed to involve templating of mesophase growth during evaporation of volatile solvents; this process, known as evaporation-induced self-assembly (EISA),[7–11] has been used broadly for the preparation of mesoporous materials. This alternative synthetic approach allows the tuning of inorganic condensation with the formation of meso-organized liquid-crystal templates.[8,12–24] As the solvent is removed, a mesophase gradually forms. Because the majority of amphiphilic diblock copolymers are water-insoluble, the EISA strategy has become very useful when fabricating various mesoporous nanostructures having large pores. Several synthetic strategies have been developed based on poly(ethylene oxide)-*b*-poly(propylene oxide)-*b*-poly(ethylene oxide) (PEO-PPO-PEO) triblock copolymers as templates, allowing the preparation of many highly ordered large-pore mesoporous materials.[3,4,17,21,23,25–44]

The EISA strategy involves templating of the mesophase growth during evaporation of a volatile solvent. As a result, it is important to have control over the rate of solvent evaporation; for example, when preparing long-range-ordered mesoporous materials through a spray drying method.[45] Recently, Choi *et al.*[46] found that relatively hydrophobic 1-butanol, when compared with EtOH, enhanced the phase separation between water and the PEO-PPO-PEO triblock copolymer (template). In addition, Hu *et al.*[47] reported microstructural tuning of mesoporous silicas prepared through EISA templated by Pluronic F127 ($PEO_{106}$-$PPO_{70}$-$PPO_{106}$) in various solvents, including MeOH, EtOH, *n*-propanol, *n*-butanol, and tetrahydrofuran (THF). They proposed that the rate of self-assembly relative to the rate of silica precursor condensation depended strongly on the rate of solvent evaporation. In other words, the rate of evaporation of the solvent is the key factor determining the resultant microstructure of silica templates synthesized

*Department of Materials and Optoelectronic Science, Center for Functional Polymers and Supramolecular Materials, National Sun Yat-Sen University, Kaohsiung, 804, Taiwan. E-mail: kuosw@faculty.nsysu.edu.tw*

through EISA. However, commercially available PEO-PPO-PEO triblock copolymers are seldom able to directly template ordered mesoporous silicas with pore sizes larger than 12 nm because of molecular weight and composition limitations.

In previous studies,[48,49] we used a series of amphiphilic poly(ethylene oxide-*b*-ε-caprolactone) (PEO-*b*-PCL) block copolymers of various molecular weights as templates to prepare ordered mesoporous silica materials, observing transformations of the morphology upon varying the weight fractions of tetraethyl orthosilicate (TEOS) and the template. PEO-*b*-PCL block copolymer could easily be synthesized and controlled molecular weight to prepare difference pore size materials and PEO-*b*-PCL have a high biocompatibility and can be degraded. We also examined the effect of the molecular weight of the templating PEO-*b*-PCL on the fabrication of ordered mesoporous phenolic resins[50–52] and polybenzoxazines.[53] In each of those studies, we selected THF as the solvent for preparing the mesoporous materials because it solubilizes both PEO and PCL block segments. For this present study, we prepared mesoporous silicas through EISA, templated by the diblock copolymer PEO-*b*-PCL, in various solvents, including $CH_2Cl_2$, THF, and acetone. We used small-angle X-ray scattering (SAXS), transmission electron microscopy (TEM), and $N_2$ adsorption/desorption isotherms to investigate the phase behavior of the resulting mesoporous silicas. In addition, this work has potential applications not only drug release but also solar cell.

# Experimental

### Materials

Monomethoxy-poly(ethylene glycol) having a molecular weight of 5000 ($EO_{114}$, Aldrich) was obtained from Aldrich and dried through azeotropic distillation with dry toluene. ε-caprolactone (ε-CL, 99%, Acros) was purified through vacuum distillation over $CaH_2$ (93%, Acros); the distillation fraction collected at 96–98 °C (5 mm-Hg) was used in all polymerization reactions. Stannous(ii) octoate [$Sn(Oct)_2$, 96%, Alfa Aesar] was used as received. The double-crystalline block copolymer PEO-*b*-PCL ($EO_{114}CL_{84}$) was synthesized through ring-opening polymerization; it had a molecular weight of 14 580 g $mol^{-1}$ (determined using $^1H$ NMR spectroscopy) and a polydispersity index (PDI) of 1.31 [determined using gel permeation chromatography (GPC) with *N*,*N*-dimethylformamide (DMF) as the eluent (0.6 mL $min^{-1}$) and calibration with polystyrene (PS) standards]. $CH_2Cl_2$, THF, acetone, TEOS, and HCl (all from Aldrich) were used as received. Deionized water was used in all experiments.

### Synthesis of mesoporous silicas

Mesoporous silicas were prepared using an EISA strategy in a solvent containing the PEO-*b*-PCL as the template and TEOS as the silica precursor. Prior to direct calcination, hydrothermal treatment was applied. In a typical synthetic procedure, TEOS (0.1 g) and 0.1 M HCl (0.10 g) were added to a solvent ($CH_2Cl_2$, THF, or acetone; 5 g) containing PEO-*b*-PCL and stirred for 30 min to form a homogeneous solution. The solution was poured into a Petri dish and then the solvent was evaporated at room temperature for 48 h. The transparent film was collected and ground into a powder, which was transferred into a PFA bottle containing 1.0 M HCl (30 mL) and hydrothermally treated at 100 °C for 3 days. The product was washed with water and EtOH, dried at room temperature, and calcined in air at 500 °C to produce a white mesoporous silica; the calcination was conducted in a furnace operated at a heating rate of 2 °C $min^{-1}$.

### Characterization

SAXS data were recorded using a NANOSTAR U small-angle X-ray scattering system (Bruker AXS, Karlsruhe, Germany) and Cu Kα radiation (30 W, 50 kV, 600 μA). The *d*-spacings were calculated using the formula $d = 2\pi/q$, where $q$ is the scattering vector. TEM images were recorded using a JEOL 3010 microscope operated at 200 kV; samples for TEM measurement were suspended in EtOH and supported onto a holey carbon film on a Cu grid. Nitrogen adsorption/desorption isotherms were measured at −196 °C using an ASAP 2020 analyzer; prior to measurements, the samples were degassed under vacuum at 300 °C for at least 6 h. The Brunauer–Emmett–Teller (BET) method was used to calculate the specific surface areas and pore volumes; pore size distributions were derived from the adsorption branches of the isotherms by applying the Barrett–Joyner–Halenda (BJH) model.

# Results and discussion

### Mesoporous silicas prepared at various TEOS/PEO-*b*-PCL ratios in $CH_2Cl_2$

We prepared the mesoporous silica samples D1–D5 (solvent: $CH_2Cl_2$), T1–T5 (solvent: THF), and A1–A5 (solvent: acetone) by employing the diblock copolymer PEO-*b*-PCL as the template at TEOS/PEO-*b*-PCL ratios of 1 : 1, 2 : 1, 3 : 1, 4 : 1, and 5 : 1, respectively.

Fig. 1 displays the SAXS patterns of samples D1–D5; the *d*-spacings of the mesoporous silicas were not represented by obvious peaks, with a broad primary scattering peak appearing when the TEOS/PEO-*b*-PCL weight ratio was in the range from 3 : 1 to 5 : 1 (D3–D5). In agreement, TEM images [Fig. 1(b)–(f)] revealed morphologies displaying slit-like pores for samples D1–D5. According the BDDT (Brunauer, Deming, Deming, and Teller) classification system, the mesoporous silica samples D1–D5 all provided typical type-IV isotherms in their $N_2$ adsorption/desorption curves [Fig. 2(a)]. According the IUPAC definition, the isotherm of D1 exhibited $H_3$-like hysteresis loops (slit-like) at values of $P/P_0$ ranging from 0.80 to 1.00, indicative of a typical mesoporous structure having slit-like pores. When we increased the TEOS/PEO-*b*-PCL weight ratio, forming D2, we again noted $H_3$-like hysteresis loops (slit-like) in the relative pressure ($P/P_0$) range between 0.42 and 0.90, with no obvious distribution of pore sizes [Fig. 2(b)]. The hysteresis loops of D3–D5 were also $H_3$-like (slit-like) in the relative pressure ($P/P_0$) range between 0.42 and 1.00, with pore sizes of 7.8, 6.7, and 9.0 nm, respectively. Fig. 2(b) displays the mean pore sizes measured from the adsorption branches, based on the Harkins–Jura model. The mesopore pore size distributions were quite

uniform, at approximately about 8.0 nm, for samples D3–D5, which exhibited slit-like morphologies [TEM images in Fig. 1(b)–(f)].

### Mesoporous silicas prepared at various TEOS/PEO-*b*-PCL ratios in THF

To study the effect of solvent on the EISA process for the synthesis of mesoporous silicas templated by the diblock copolymer PEO-*b*-PCL, we recorded SAXS patterns [Fig. 3(a)] and TEM images [Fig. 3(b)–(f)] of mesoporous silicas prepared at various TEOS/PEO-*b*-PCL weight ratios in THF. The SAXS patterns featured an obvious broad first-order scattering peak at a value of $q$ of 0.17 $nm^{-1}$ when the TEOS/PEO-*b*-PCL ratio was 1 : 1, suggesting disordered micelles or a slit-like structure, which we confirmed through TEM imaging [Fig. 3(b)]. In contrast, the SAXS pattern featured its maximum intensity at a value of $q$ of 0.24 $nm^{-1}$ ($d = 38.3$ nm) and another peak at $3^{1/2}q^*$ when the TEOS/PEO-*b*-PCL ratio was 2 : 1, indicating the short range order of a hexagonal packing cylinder structure, as confirmed by TEM imaging [Fig. 3(c)]. Further increasing the TEOS/PEO-*b*-PCL weight ratio to 3 : 1 (T3), 4 : 1 (T4), and 5 : 1 (T5) caused the primary SAXS peaks to gradually sharpen with higher-order reflections at $3^{1/2}q^*$, $2q^*$, and $7^{1/2}q^*$, indicating that these mesoporous silicas became more ordered with the long range order of hexagonally packed cylinder structures. These features were also evident in the TEM images [Fig. 3(d)–(f)], with that and of T4 [Fig. 3(e)] revealing a hexagonally packed cylinder structure of relatively high long-range-order.

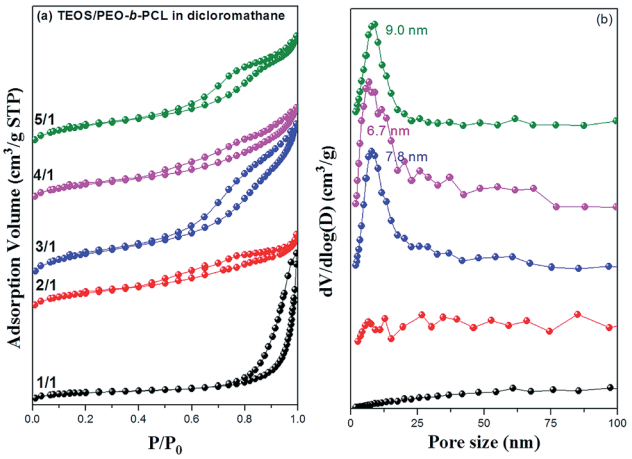


Fig. 2 (a) $N_2$ adsorption/desorption isotherms and (b) pore size distribution curves of mesoporous silicas templated by PEO-*b*-PCL in $CH_2Cl_2$.

Fig. 4 presents $N_2$ sorption isotherms of the mesoporous silicas prepared at the various TEOS/PEO-*b*-PCL weight ratios in THF; we observe representative type-IV curves according the BDDT classification system. Sample T1 underwent a capillary condensation step in the relative pressure range from 0.6 to 1.0 [Fig. 4(a)], thereby exhibiting a typical $H_3$-like hysteresis loop, characteristic of slit-like mesopores, indicating a broad pore size distribution centered near 32.9 nm [Fig. 4(b)], based on the Harkins–Jura model. Sample T2 revealed an $H_1$-like hysteresis

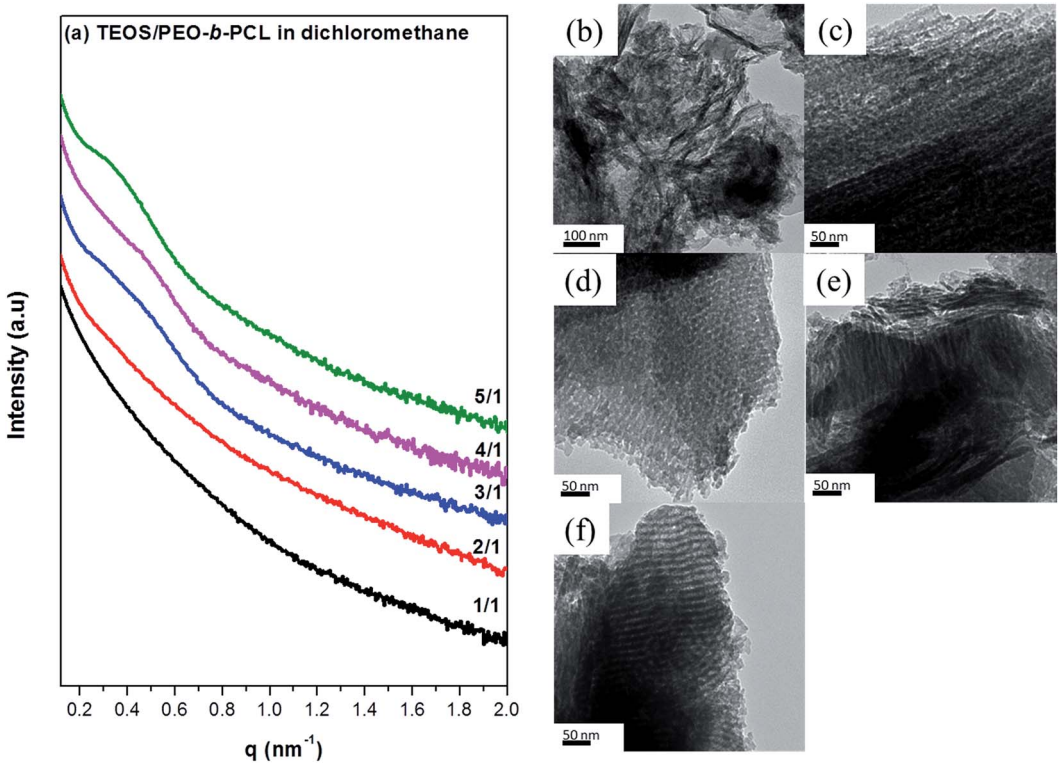


Fig. 1 (a) SAXS patterns and (b–f) TEM images of mesoporous silicas templated by PEO-*b*-PCL in $CH_2Cl_2$ at TEOS/PEO-*b*-PCL weight ratios of (b) 1 : 1, (c) 2 : 1, (d) 3 : 1, (e) 4 : 1, and (f) 5 : 1.

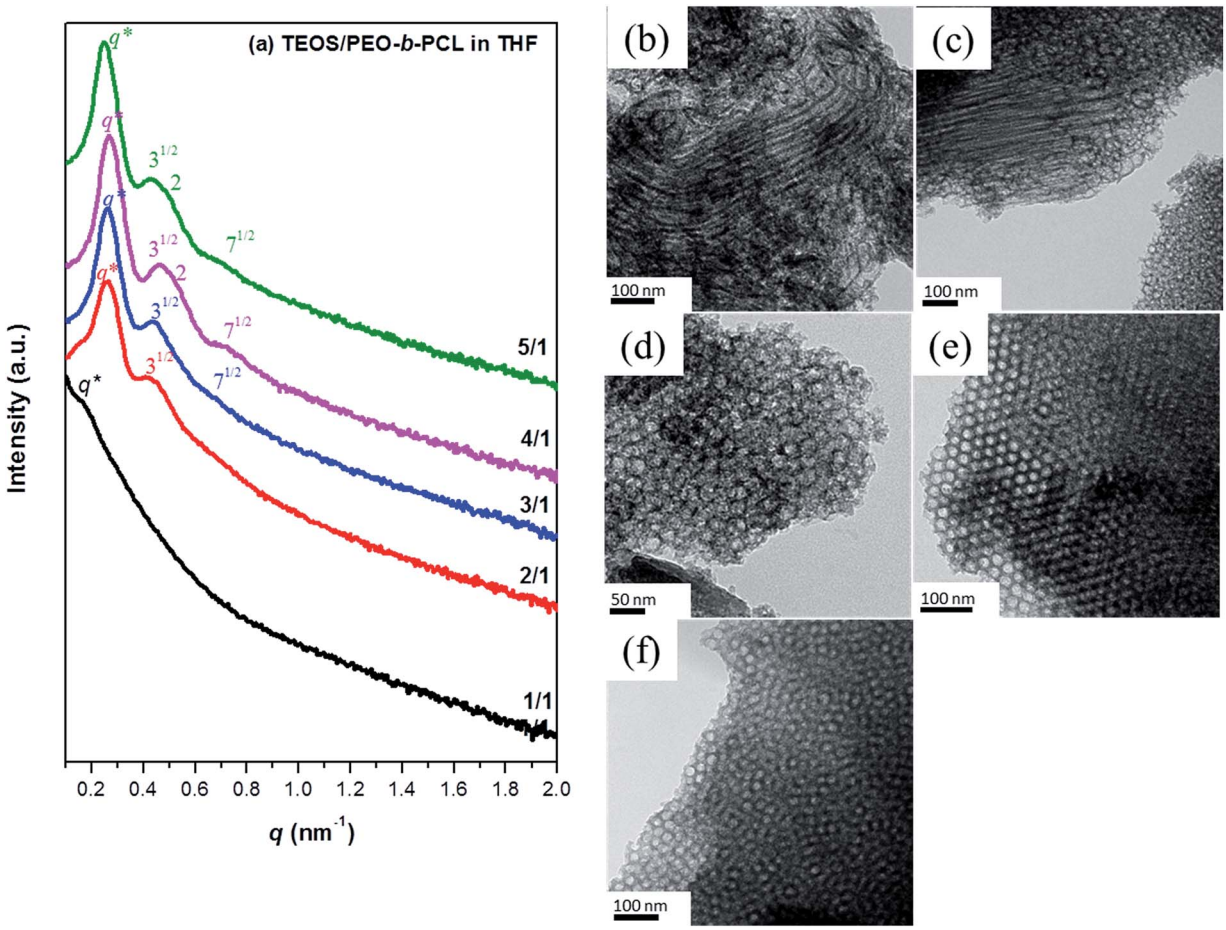


Fig. 3 (a) SAXS patterns and (b–g) TEM images of mesoporous silicas templated by PEO-*b*-PCL in THF at TEOS/PEO-*b*-PCL weight ratios of (b) 1 : 1, (c) 2 : 1, (d) 3 : 1, (e) 4 : 1, and (f) 5 : 1.

loop at values of $P/P_0$ from 0.42 to 1.00, suggesting a change from disordered micelles to a cylindrical mesoporous structure. Increasing the TEOS content resulted in samples T3–T5 exhibiting typical $H_2$-like hysteresis loops, characteristic of spherical mesopores. The pore size distribution curves revealed that samples T3–T5 featured average pore sizes of approximately 17–19 nm.

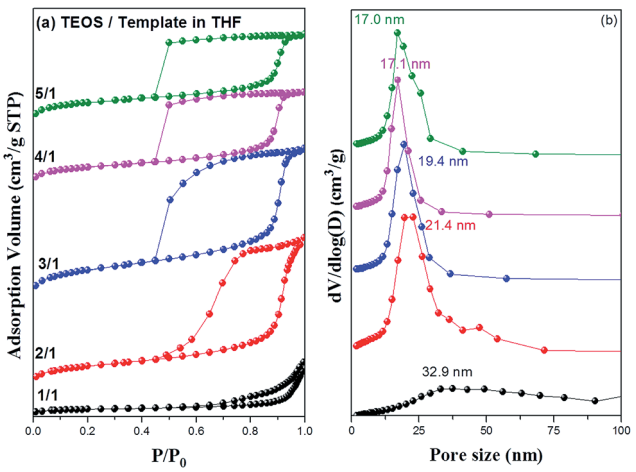


Fig. 4 (a) $N_2$ adsorption/desorption isotherms and (b) pore size distribution curves of mesoporous silicas templated by PEO-*b*-PCL in THF.

### Mesoporous silicas prepared at various TEOS/PEO-*b*-PCL ratios in acetone

Next, we investigated the effect of acetone as the solvent for the synthesis of mesoporous silicas through EISA in the presence of PEO-*b*-PCL. We recorded SAXS patterns [Fig. 5(a)] and TEM images [Fig. 5(b)–(f)] of the mesoporous silicas templated by PEO-*b*-PCL at various TEOS/PEO-*b*-PCL weight ratios in acetone. The SAXS pattern of the sample prepared at a TEOS/PEO-*b*-PCL ratio of 1 : 1 featured a signal at a value of $q^*$ of 0.19 $nm^{-1}$ ($d$ = 34.6 nm) with corresponding peaks at $3^{1/2}q^*$ and $7^{1/2}q^*$, indicating a hexagonally packed cylinder structure, which was confirmed by the TEM image. Relative to the samples prepared at the same TEOS/PEO-*b*-PCL ratio (1 : 1) in $CH_2Cl_2$ and THF, higher-order peaks appeared when acetone was the solvent. Thus, this mesoporous silica became more ordered, from a disordered micelle structure to a cylinder structure, upon changing the solvent from THF to acetone. Further increasing the TEOS/PEO-*b*-PCL weight ratio

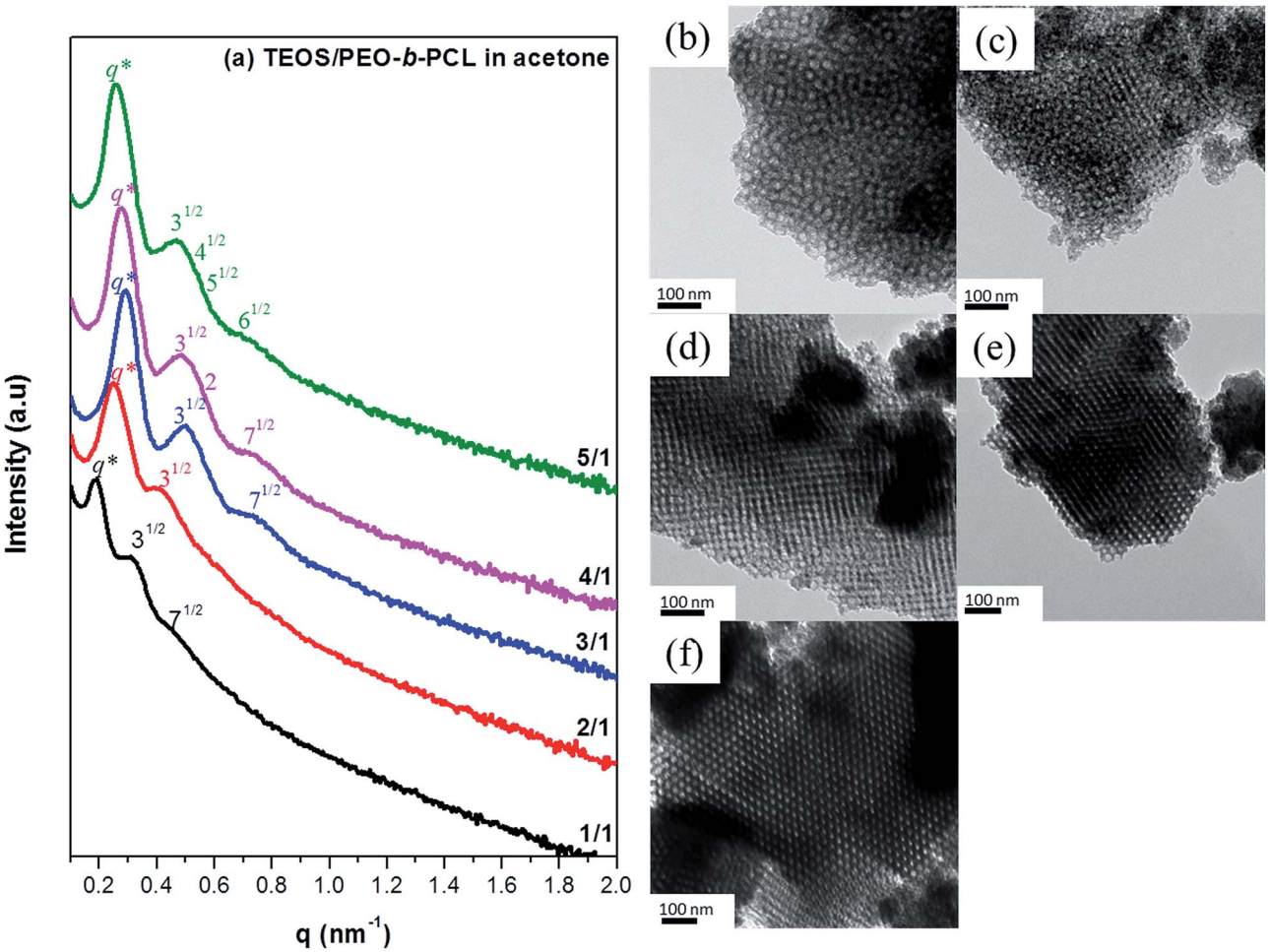


Fig. 5 (a) SAXS patterns and (b–g) TEM images of mesoporous silicas templated by PEO-*b*-PCL in acetone at TEOS/PEO-*b*-PCL weight ratios of (b) 1 : 1, (c) 2 : 1, (d) 3 : 1, (e) 4 : 1, and (f) 5 : 1.

to 2 : 1 (A2), 3 : 1 (A3), 4 : 1 (A4), and 5 : 1 (A5) caused the SAXS peaks to gradually sharpen with higher-order reflections at $3^{1/2}q^*$, $4^{1/2}q^*$, $5^{1/2}q^*$, $6^{1/2}q^*$, and $7^{1/2}q^*$. TEM images revealed that these mesoporous silicas became more ordered, with the long-range order of hexagonally packed cylinder structures for A2–A4 [Fig. 5(c)–(e)] to a body-centered cubic (bcc-type) structure for A5 [Fig. 5(f)]. According to the BDDT classification system, the $N_2$ sorption isotherms exhibited (Fig. 6) typical type-IV curves. For sample A1, prepared at a TEOS/PEO-*b*-PCL ratio of 1 : 1, we observed a sharp capillary condensation in the relative pressure range between 0.6 and 1.0, with $H_1$-like hysteresis loops [Fig. 6(a)] and a pore size distribution centered at 40 nm [Fig. 6(b)]. For sample A2, prepared at a TEOS/PEO-*b*-PCL ratio of 2 : 1, we also observed a sharp capillary condensation in the relative pressure range between 0.5 and 1.0, with $H_1$-like hysteresis loops and a pore size distribution centered at 22.7 nm [determined using the Broekhoff–de Boer (BdB) model]. The other mesoporous silica samples (A3–A5) exhibited sharp capillary condensation steps in the relative pressure range from 0.45 to 0.90, with $H_2$-like hysteresis loops characteristic of spherical mesopores; the pore size distributions, derived from the adsorption branches, narrowed significantly, to approximately 18 nm (determined using the BdB model).

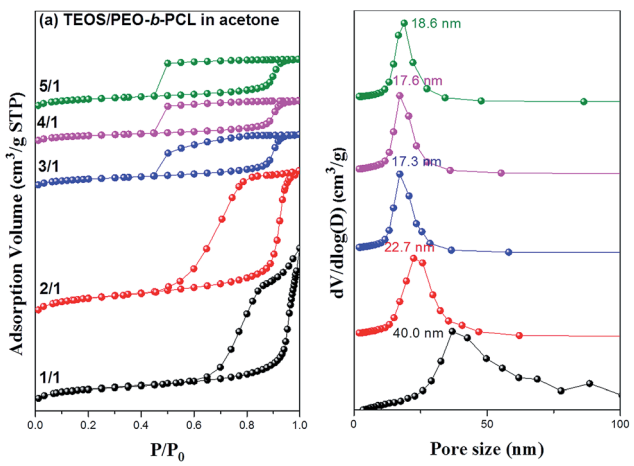


Fig. 6 (a) $N_2$ adsorption/desorption isotherms and (b) pore size distribution curves of mesoporous silicas templated by PEO-*b*-PCL in acetone.

Furthermore, we were interested in further studying the bcc mesoporous silica of sample A5. Fig. 7(a) displays its SAXS pattern, featuring a strong reflection having a *d*-spacing of 25.1 nm, with two strong reflections at values of $q$ of 0.25 and 0.45 $nm^{-1}$; this SAXS pattern could be indexed as having (110), (211), and (220) reflections, corresponding to the space group *Im3m*. In addition, we confirmed the cubic symmetry and structural ordering of this material through TEM analyses. Fig. 7(b)–(d) display TEM images of the bcc-type mesoporous silica material in different orientations ([100], [110], and [111] planes, respectively). We obtained further information regarding the textural properties of the materials from $N_2$ adsorption/desorption isotherms measured at −196 °C. Fig. 7(e) presents the $N_2$ sorption isotherms of the cubic mesoporous silica sample. The sample displays individual type-IV isotherms according the BDDT classification system, exhibiting the apparent $H_2$ hysteresis loop characteristics of a cage-like mesoporous material. A sharp capillary condensation step appeared for this sample, suggesting high-quality ordering and uniform pore dimensions, in agreement with the SAXS pattern and TEM images. Pore size distribution analysis revealed [Fig. 7(f)] a well-ordered cubic structure having pores with an average diameter of approximately 18.6 nm. Table 1 summarizes the BET surface areas, pore volumes, and BJH pore sizes of the mesoporous silica materials prepared in this study when using $CH_2Cl_2$, THF, and acetone as solvents.

### Effect of solvent on mesoporous silicas prepared at a TEOS/PEO-*b*-PCL ratio of 5 : 1

Fig. 8 presents SAXS patterns and TEM images of the mesoporous silicas we prepared from various solvents while keeping the TEOS-to-template ratio constant at 5 : 1. The SAXS pattern of sample D5 featured no obvious peaks and only a broad primary scattering peak. Samples T5 and A5 provided similar, well-resolved SAXS peaks [Fig. 8(a)] at values of $q^*$ of 0.26 $nm^{-1}$ ($d$ = 24.2 nm) and 0.25 $nm^{-1}$ ($d$ = 25.1 nm), respectively. The SAXS profile of sample A5 exhibited [Fig. 8(a)] organized peaks ($q^*$ = 0.25 $nm^{-1}$; $d$ = 25.1 nm) having a peak ratio of $1 : 3^{1/2} : 4^{1/2} : 5^{1/2}$. The SAXS pattern and TEM images (Fig. 7) already suggested a clear bcc structure. The TEM images of samples D5 and T5 [Fig. 8(b) and (c), respectively] revealed slit-like pores and hexagonally packed cylindrical pores, respectively. Fig. 9 presents $N_2$ sorption isotherms of the mesoporous silica samples prepared at a TEOS/PEO-*b*-PCL weight ratio of 5 : 1 in the various solvents. According to the BDDT

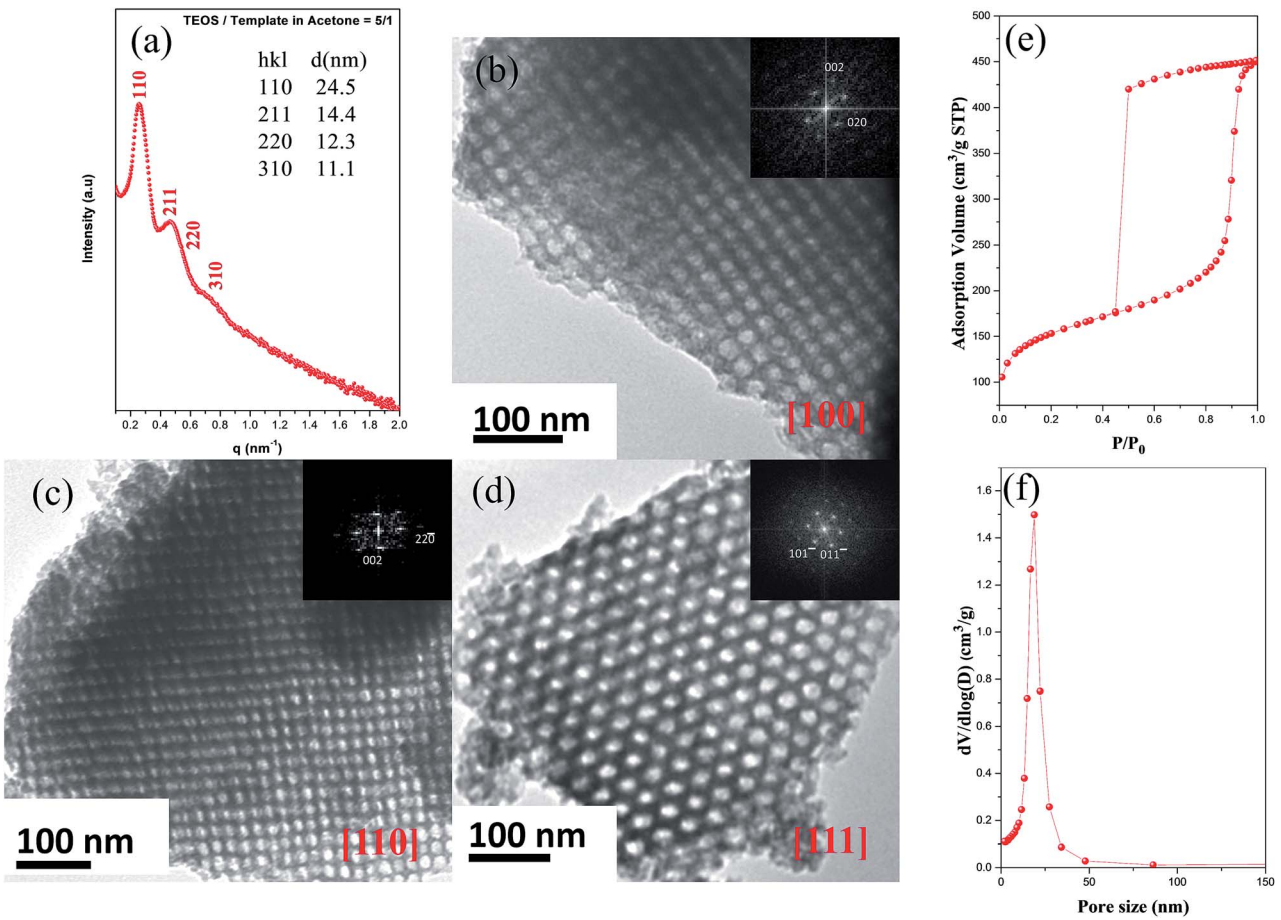


Fig. 7 (a) SAXS pattern, (b–d) TEM images viewed from the (b) [100], (c) [110], and (d) [111] planes (insets: corresponding FFT), (e) $N_2$ adsorption/desorption isotherm, and (f) pore size distribution curve of the bcc mesoporous silica templated by PEO-*b*-PCL at a TEOS/PEO-*b*-PCL ratio of 5 : 1 in acetone.

Table 1 Textural properties of mesoporous silicas templated by the diblock copolymer PEO-*b*-PCL in various solvents

| Sample | TEOS/Template | Solvent | $d^a$ (nm) | Pore size (nm) | $^bS_{BET}$ ($m^2\ g^{-1}$) | $^bS_M$ ($m^2\ g^{-1}$) | Pore volume ($cm^3\ g^{-1}$) | Micropore volume ($cm^3\ g^{-1}$) |
|---|---|---|---|---|---|---|---|---|
| D1 | 1 : 1 | $CH_2Cl_2$ | — | — | 256.9 | 63.1 | 1.47 | 0.026 |
| D2 | 2 : 1 | $CH_2Cl_2$ | — | — | 185.5 | 116.4 | 0.18 | 0.051 |
| D3 | 3 : 1 | $CH_2Cl_2$ | — | 7.8 | 406.7 | 97.1 | 0.68 | 0.041 |
| D4 | 4 : 1 | $CH_2Cl_2$ | — | 6.7 | 258.9 | 50.2 | 0.41 | 0.021 |
| D5 | 5 : 1 | $CH_2Cl_2$ | — | 9.0 | 323.8 | 71.4 | 0.49 | 0.030 |
| T1 | 1 : 1 | THF | 38.3 | 32.9 | 102.6 | 33.1 | 0.35 | 0.014 |
| T2 | 2 : 1 | THF | 25.1 | 21.4 | 396.8 | 80.0 | 1.00 | 0.033 |
| T3 | 3 : 1 | THF | 23.8 | 19.4 | 585.9 | 136.3 | 1.04 | 0.058 |
| T4 | 4 : 1 | THF | 23.5 | 17.1 | 424.0 | 156.4 | 0.67 | 0.070 |
| T5 | 5 : 1 | THF | 24.2 | 17.0 | 475.8 | 184.9 | 0.65 | 0.082 |
| A1 | 1 : 1 | Acetone | 34.6 | 40.0 | 580.3 | 99.8 | 1.89 | 0.039 |
| A2 | 2 : 1 | Acetone | 24.6 | 22.7 | 848.2 | 250.2 | 1.85 | 0.109 |
| A3 | 3 : 1 | Acetone | 21.5 | 17.3 | 430.6 | 145.2 | 0.71 | 0.064 |
| A4 | 4 : 1 | Acetone | 23.0 | 17.6 | 412.3 | 185.8 | 0.59 | 0.084 |
| A5 | 5 : 1 | Acetone | 25.1 | 18.6 | 534.0 | 237.3 | 0.69 | 0.107 |

[a] The *d*-spacings were calculated from the first SAXS peak, using the formula $d = 2\pi/q^*$. [b] $S_{BET}$ and $S_M$ are the total BET surface area and the micropore surface area calculated from the *t*-plots, respectively.

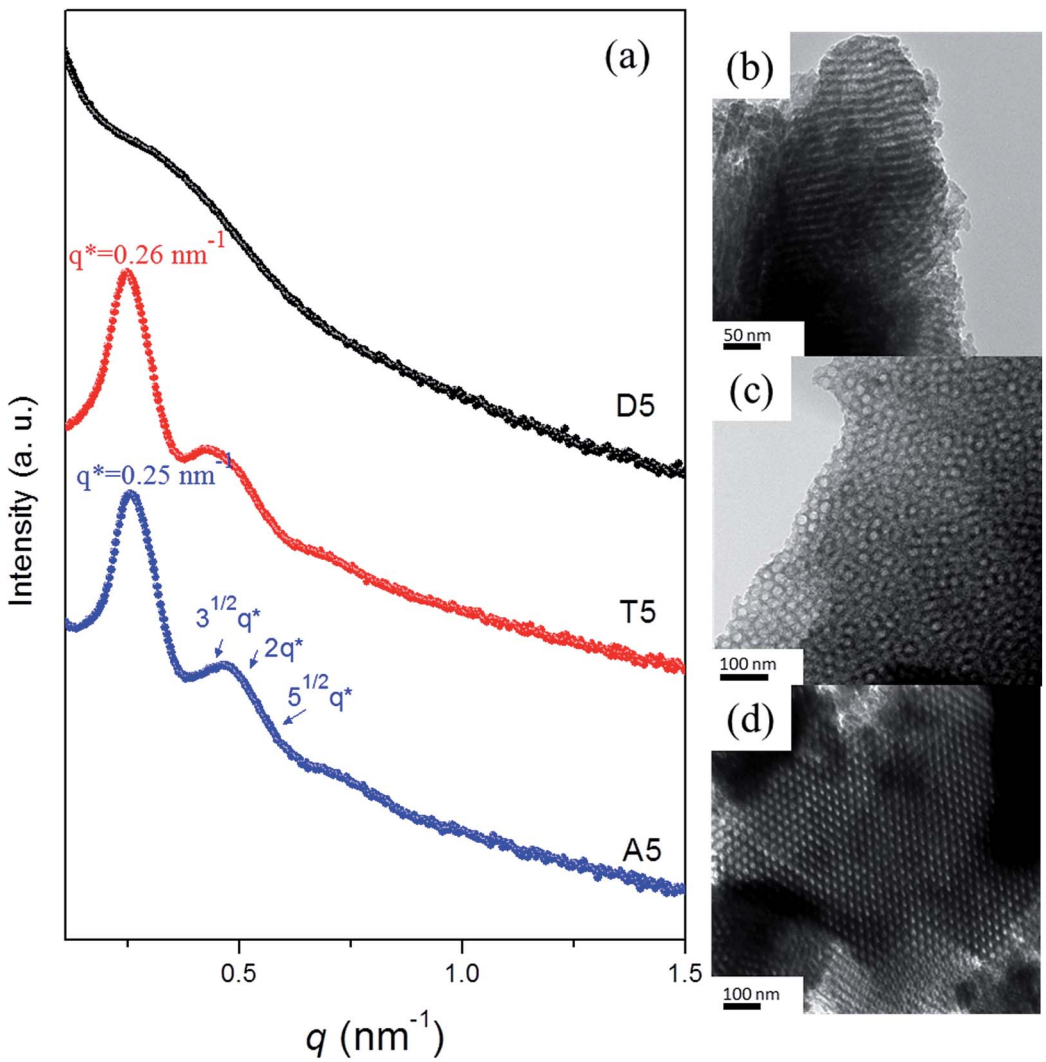


Fig. 8 (a) SAXS patterns and (b–d) TEM images of mesoporous silicas templated by PEO-*b*-PCL at a TEOS/PEO-*b*-PCL ratio of 5 : 1 in (b) $CH_2Cl_2$, (c) THF, and (d) acetone.

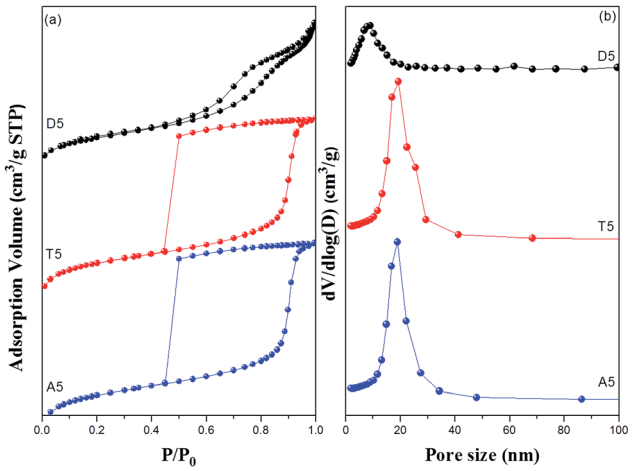


Fig. 9 (a) $N_2$ adsorption/desorption isotherms and (b) pore size distribution curves of mesoporous silicas templated by PEO-*b*-PCL at a TEOS/PEO-*b*-PCL ratio of 5 : 1 in various solvents.

classification system, they all display type-IV isotherms, with the mesoporous silica samples T5 and A5 exhibiting sharp capillary condensation steps in the relative pressure range from 0.45 to 0.90, with $H_2$-like hysteresis loops characteristic of spheres, while the other mesoporous silica sample, D5, exhibited a sharp capillary condensation step in the relative pressure range from 0.42 to 1.0 with $H_1$-like hysteresis loops characteristic of the slit-like structure displayed in Fig. 8(b).

On the basis of these results, we speculate that $CH_2Cl_2$ is not a good solvent, but THF and acetone are, for the preparation of mesoporous silicas templated by the diblock copolymer PEO-*b*-PCL. Table 2 summarizes the physical properties of $CH_2Cl_2$, THF, and acetone. In addition, the solubility parameters of PEO and PCL are both equal to 9.4 $(\text{cal mL}^{-1})^{1/2}$, based on the calculation from group contribution method.[54] Among our three tested solvents, $CH_2Cl_2$ has the fastest evaporation rate (lowest boiling temperature and highest vapor pressure) and largest solubility parameter difference with the block copolymer PEO-*b*-PCL; thus, it induced mesoporous silicas having short-range order when templated by PEO-*b*-PCL. Although the rate of evaporation of acetone is fast relative to that of THF, its solubility is better than that of THF because the solubility parameters of acetone are equal to those of the PEO and PCL block segments. Polymer solution theory suggests that a chain will be more expanded in the presence of a good solvent. In addition, the chain will swell in a good solvent to maximize the number of polymer fluid contacts; for a bad solvent, the chain segments will shrink. As a result, the sizes of the mesopores in the mesoporous silicas generally followed the order acetone > THF > $CH_2Cl_2$ (Table 1), consistent with the solvent solubilities of the block copolymer PEO-*b*-PCL. In addition, because of their different solubilities, the three solvents provided different mesoporous structures; for example, the T5 sample featured hexagonally packed cylinders and the A5 sample featured bcc spheres. All the possible mesoporous structures templated by PEO-*b*-PCL in various solvents are summarized in Scheme 1.

Table 2 Physical properties of solvents used in this study

| | $CH_2Cl_2$ | THF | Acetone |
|---|---|---|---|
| Molar mass | 84.93 g $mol^{-1}$ | 72.11 g $mol^{-1}$ | 58.08 g $mol^{-1}$ |
| Density | 1.3255 g $cm^{-3}$ | 0.8892 g $cm^{-3}$ | 0.79 g $cm^{-3}$ |
| Boiling point | 39 °C | 66 °C | 56 °C |
| Solubility in water | 13 g $L^{-1}$, 20 °C | Miscible | Miscible |
| Solubility parameter | 10.3 $(\text{Cal mL}^{-1})^{0.5}$ | 8.8 $(\text{Cal mL}^{-1})^{0.5}$ | 9.4 $(\text{Cal mL}^{-1})^{0.5}$ |
| Vapor pressure | 47 kPa, 20 °C | 19.07 kPa, 20 °C | 24.46 kPa, 20 °C |

Although is well established that SBA-16 has a bcc structure, mesoporous silicas having cubic *Im*$\bar{3}$*m* structures with large pores (>10 nm) are rarely observed because the distribution of the mesophase diagram is very narrow; the soft templates require a high volume fraction of the hydrophilic segment of the block copolymer (*e.g.*, PEO segment). To date, the most studied mesoporous silica having a bcc structure displays excellent performance in various applications because of its large cage-like (or spherical) mesopores. In a previous study,[49] we prepared a series of PEO-*b*-PCL diblock copolymers that we then used to regulate the morphologies and pore sizes of mesoporous silicas through variations in the molecular weight and the hydrophilic/hydrophobic (PEO/PCL) segment ratio of the template in THF as the solvent. We found the bcc structure when employing the PEO-*b*-PCL copolymer $EO_{114}CL_{20}$, which had a large volume fraction of its EO block segment and a very small volume fraction of its CL block segment, as the template at a TEOS/PEO-*b*-PCL ratio of 2 : 1 in THF. Because of the low molecular weight of the hydrophobic segment ($M_n$ = 2000 g $mol^{-1}$ for the PCL block segment), however, the pores had an average diameter of only approximately 10.1 nm. In this present study, we used the PEO-*b*-PCL block copolymer $EO_{114}CL_{84}$ as a template to prepare a mesoporous silica at a TEOS/PEO-*b*-PCL ratio of 5 : 1 in acetone. Surprisingly, we also found the same bcc structure, but in this case it had pores with an average diameter of approximately 18.6 nm. Thus, even though the block copolymer had a relatively low volume fraction of the hydrophilic segment (PEO) and a relatively high volume fraction of the hydrophobic segment (PCL), the bcc structure was retained in this present study because of the better solubility of acetone. Because of the relatively high molecular weight of the hydrophobic segment ($M_n$ = 10 000 g $mol^{-1}$ for the PCL block segment), the average diameter of the pores increased to approximately 18.6 nm when using $EO_{114}CL_{84}$ as the PEO-*b*-PCL block copolymer. This result is very similar to that of a previous study[49] in which we added star PEO-POSS, a swelling and modification agent, to the PEO-*b*-PCL block copolymer at a TEOS/$PEO_{114}$-*b*-$PCL_{84}$/PEO-POSS ratio of 3 : 1 : 0.7; that resulting mesoporous silica also featured an ordered bcc structure with an average pore diameter of 22.6 nm. In summary, when we

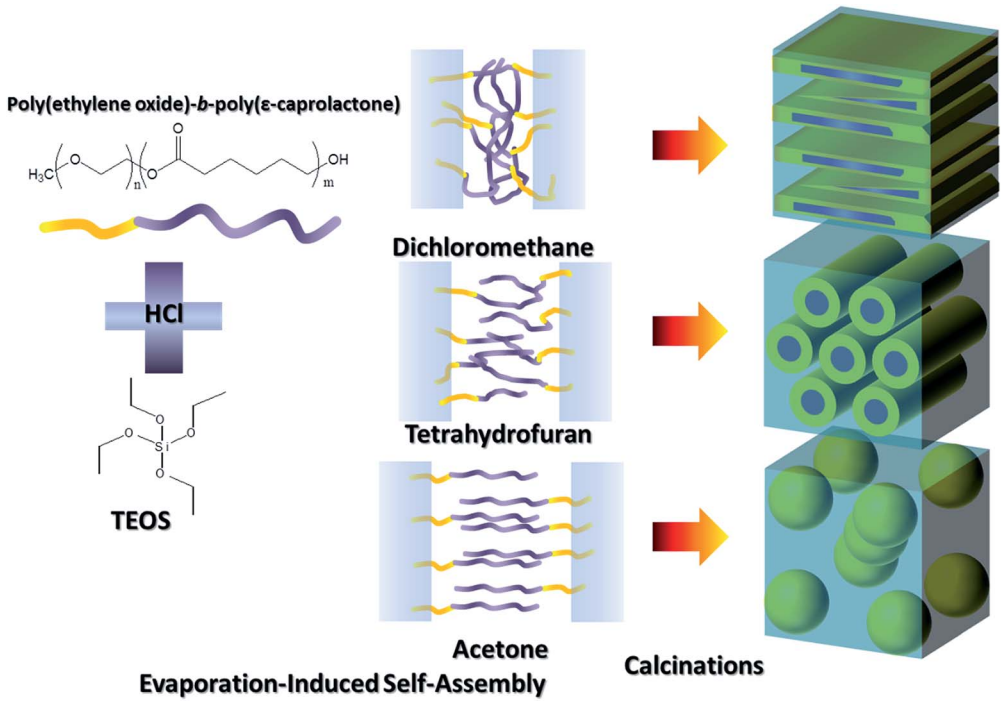


Scheme 1 Preparation of mesoporous silicas under various conditions.

chose a good solvent for the template, it performed in a manner similar to a swelling and modification agent for the template, expanding its chains and providing mesoporous materials having larger pores after calcination of the template.

## Conclusions

We have prepared mesoporous silica materials through EISA employing a PEO-*b*-PCL diblock copolymer as the template at various TEOS/PEO-*b*-PCL ratios in various solvents ($CH_2Cl_2$, THF, acetone). We found that acetone was a better solvent than either $CH_2Cl_2$ or THF because it provided better solubility for the PEO-*b*-PCL block copolymer. Structures featuring bcc mesopores of long-range order and large pores were readily prepared when using acetone as the solvent, even though the volume fraction of the hydrophobic segment was high in this template. Using this approach, we could prepare highly ordered mesoporous silicas having large pores merely through selection of an appropriate solvent; such materials might have potential applications as templates and matrices.

## Acknowledgements

This study was supported financially by the Ministry of Science and Technology, Republic of China, under contracts MOST 100-2221-E-110-029-MY3 and MOST 102-2221-E-110-008-MY3. We thank Mr Hsien-Tsan Lin of the Regional Instruments Center, National Sun Yat-Sen University, for help with the TEM experiments.

## References

1 J. S. Beck, J. C. Vartuli, W. J. Roth, M. E. Leonowicz, C. T. Kresge, K. D. Schmitt, C. T. W. Chu, D. H. Olson, E. W. Sheppard, S. B. McCullen, J. B. Higgins and J. L. Schlenker, *J. Am. Chem. Soc.*, 1992, **114**, 10834–10843.
2 C. T. Kresge, M. E. Leonowicz, W. J. Roth, J. C. Vartuli and J. S. Beck, *Nature*, 1992, **359**, 710–712.
3 D. Y. Zhao, J. L. Feng, Q. S. Huo, N. Melosh, G. H. Fredrickson, B. F. Chmelka and G. D. Stucky, *Science*, 1998, **279**, 548–552.
4 D. Y. Zhao, Q. S. Huo, J. L. Feng, B. F. Chmelka and G. D. Stucky, *J. Am. Chem. Soc.*, 1998, **120**, 6024–6036.
5 M. Kruk, M. Jaroniec, C. H. Ko and R. Ryoo, *Chem. Mater.*, 2000, **12**, 1961–1968.
6 K. C. W. Wu, X. Jiang and Y. Yamauchi, *J. Mater. Chem.*, 2011, **21**, 8934–8939.
7 G. Soler-Illia, A. Louis and C. Sanchez, *Chem. Mater.*, 2002, **14**, 750–759.
8 D. Grosso, C. Boissiere, B. Smarsly, T. Brezesinski, N. Pinna, P. A. Albouy, H. Amenitsch, M. Antonietti and C. Sanchez, *Nat. Mater.*, 2004, **3**, 787–792.
9 C. J. Brinker, Y. F. Lu, A. Sellinger and H. Y. Fan, *Adv. Mater.*, 1999, **11**, 579–585.
10 Y. F. Lu, H. Y. Fan, A. Stump, T. L. Ward, T. Rieker and C. J. Brinker, *Nature*, 1999, **398**, 223–226.
11 D. Grosso, F. Cagnol, G. Soler-Illia, E. L. Crepaldi, H. Amenitsch, A. Brunet-Bruneau, A. Bourgeois and C. Sanchez, *Adv. Funct. Mater.*, 2004, **14**, 309–322.
12 N. Hao, Y. X. Yang, H. T. Wang, P. A. Webley and D. Y. Zhao, *J. Colloid Interface Sci.*, 2010, **346**, 429–435.

13 C. J. Brinker, Y. F. Lu, A. Sellinger and H. Y. Fan, *Adv. Mater.*, 1999, **11**, 579–585.
14 Y. Deng, C. Liu, D. Gu, T. Yu, B. Tu and D. Y. Zhao, *J. Mater. Chem.*, 2008, **18**, 91–97.
15 Y. H. Deng, T. Yu, Y. Wan, Y. F. Shi, Y. Meng, D. Gu, L. J. Zhang, Y. Huang, C. Liu, X. J. Wu and D. Y. Zhao, *J. Am. Chem. Soc.*, 2007, **129**, 1690–1697.
16 Y. Huang, J. P. Yang, H. Q. Cai, Y. P. Zhai, D. Feng, Y. H. Deng, B. Tu and D. Y. Zhao, *J. Mater. Chem.*, 2009, **19**, 6536–6541.
17 Y. Meng, D. Gu, F. Q. Zhang, Y. F. Shi, L. Cheng, D. Feng, Z. X. Wu, Z. X. Chen, Y. Wan, A. Stein and D. Y. Zhao, *Chem. Mater.*, 2006, **18**, 4447–4464.
18 S. Valkama, A. Nykanen, H. Kosonen, R. Ramani, F. Tuomisto, P. Engelhardt, G. ten Brinke, O. Ikkala and J. Ruokolainen, *Adv. Funct. Mater.*, 2007, **17**, 183–190.
19 Y. Wan, Y. F. Shi and D. Y. Zhao, *Chem. Commun.*, 2007, 897–926.
20 K. Yu, A. J. Hurd, A. Eisenberg and C. J. Brinker, *Langmuir*, 2001, **17**, 7961–7965.
21 K. Kailasam, Y. S. Jun, P. Katekomol, J. D. Epping, W. H. Hong and A. Thomas, *Chem. Mater.*, 2010, **22**, 428–434.
22 J. Y. Zhang, Y. H. Deng, J. Wei, Z. K. Sun, D. Gu, H. Bongard, C. Liu, H. H. Wu, B. Tu, F. Schuth and D. Y. Zhao, *Chem. Mater.*, 2009, **21**, 3996–4005.
23 R. L. Liu, Y. F. Shi, Y. Wan, Y. Meng, F. Q. Zhang, D. Gu, Z. X. Chen, B. Tu and D. Y. Zhao, *J. Am. Chem. Soc.*, 2006, **128**, 11652–11662.
24 C. Liu, Y. H. Deng, J. Liu, H. H. Wu and D. Y. Zhao, *Microporous Mesoporous Mater.*, 2008, **116**, 633–640.
25 X. Y. Bao, X. S. Zhao, X. Li, P. A. Chia and J. Li, *J. Phys. Chem. B*, 2004, **108**, 4684–4689.
26 L. Cao and M. Kruk, *Colloids Surf., A*, 2010, **357**, 91–96.
27 J. P. Hanrahan, A. Donovan, M. A. Morris and J. D. Holmes, *J. Mater. Chem.*, 2007, **17**, 3881–3887.
28 S. S. Kim, A. Karkamkar, T. J. Pinnavaia, M. Kruk and M. Jaroniec, *J. Phys. Chem. B*, 2001, **105**, 7663–7670.
29 T. W. Kim, F. Kleitz, B. Paul and R. Ryoo, *J. Am. Chem. Soc.*, 2005, **127**, 7601–7610.
30 B. Z. Tian, X. Y. Liu, Z. D. Zhang, B. Tu and D. Y. Zhao, *J. Solid State Chem.*, 2002, **167**, 324–329.
31 D. H. Chen, Z. W. Li, Y. X. J. Tu, Y. F. Shi, Z. X. Chen, W. Shen, C. Z. Yu, B. Tu and D. Y. Zhao, *J. Mater. Chem.*, 2006, **16**, 1511–1519.
32 J. Lee, J. Kim, Y. Lee, S. Yoon, S. M. Oh and T. Hyeon, *Chem. Mater.*, 2004, **16**, 3323–3330.
33 Z. Y. Wang and A. Stein, *Chem. Mater.*, 2008, **20**, 1029–1040.
34 F. Q. Zhang, Y. Meng, D. Gu, Y. Yan, Z. X. Chen, B. Tu and D. Y. Zhao, *Chem. Mater.*, 2006, **18**, 5279–5288.
35 J. Tang, Y. B. Fan, J. Hu and H. L. Liu, *J. Colloid Interface Sci.*, 2009, **331**, 191–195.
36 L. Y. Song, D. Feng, C. G. Campbell, D. Gu, A. M. Forster, K. G. Yager, N. Fredin, H. J. Lee, R. L. Jones, D. Y. Zhao and B. D. Vogt, *J. Mater. Chem.*, 2010, **20**, 1691–1701.
37 C. Urata, Y. Tamura, Y. Yamauchi and K. Kuroda, *J. Mater. Chem.*, 2011, **21**, 3711–3717.
38 G. W. Zhou, Y. J. Chen, J. H. Yang and S. H. Yang, *J. Mater. Chem.*, 2007, **17**, 2839–2844.
39 H. P. Lin, C. Y. Chang-Chien, C. Y. Tang and C. Y. Lin, *Microporous Mesoporous Mater.*, 2006, **93**, 344–348.
40 M. H. Sorensen, R. W. Corkery, J. S. Pedersen, J. Rosenholm and P. C. Alberius, *Microporous Mesoporous Mater.*, 2008, **113**, 1–13.
41 L. M. Wang, B. Z. Tian, J. Fan, X. Y. Liu, H. F. Yang, C. Z. Yu, B. Tu and D. Y. Zhao, *Microporous Mesoporous Mater.*, 2004, **67**, 123–133.
42 J. F. Yao, H. T. Wang, K. Y. Chan, L. X. Zhang and N. P. Xu, *Microporous Mesoporous Mater.*, 2005, **82**, 183–189.
43 F. Q. Zhang, Y. Yan, Y. Meng, Y. Xia, B. Tu and D. Y. Zhao, *Microporous Mesoporous Mater.*, 2007, **98**, 6–15.
44 W. C. Chu, S. F. Chiang, J. G. Li and S. W. Kuo, *RSC Adv.*, 2013, **4**, 784–793.
45 I. V. Melnyk, Y. L. Zub, E. Veron, D. Massiot, T. Cacciaguerra and B. Alonso, *J. Mater. Chem.*, 2008, **18**, 1368–1382.
46 S. Y. Choi, M. Mamak, N. Coombs, N. Chopra and G. A. Ozin, *Adv. Funct. Mater.*, 2004, **14**, 335–344.
47 Y. F. Lee, K. H. Chang, C. Y. Chu, H. L. Chen and C. C. Hu, *RSC Adv.*, 2011, **1**, 401–407.
48 J. G. Li and S. W. Kuo, *RSC Adv.*, 2011, **1**, 1822–1833.
49 J. G. Li, Y. H. Chang, Y. S. Lin and S. W. Kuo, *RSC Adv.*, 2012, **2**, 12973–12982.
50 J. G. Li, Y. D. Lin and S. W. Kuo, *Macromolecules*, 2011, **44**, 9295–9309.
51 J. G. Li, W. C. Chu, U. Jeng and S. W. Kuo, *Macromol. Chem. Phys.*, 2013, **214**, 2115–2123.
52 J. G. Li, C. Y. Chung and S. W. Kuo, *J. Mater. Chem.*, 2012, **22**, 18583–18595.
53 W. C. Chu, J. G. Li and S. W. Kuo, *RSC Adv.*, 2013, **3**, 6485–6498.
54 M. M. Coleman, and P. C. Painter, *Miscible Polymer Blend-Background and Guide for Calculations and Design*, DEStech Publications, Inc., Lancaster, PA, 2006.